Editors' Suggestion

Growth and prediction of plastic strain in metallic glasses

Tero Mäkinen [1,*] Anshul D. S. Parmar [2,†] Silvia Bonfanti [2,3] and Mikko J. Alava [1,2]

[1]*Department of Applied Physics, Aalto University, P. O. Box 15600, 00076 Aalto, Espoo, Finland*

[2]*NOMATEN Centre of Excellence, National Center for Nuclear Research, ul. A. Soltana 7, 05-400 Swierk/Otwock, Poland*

[3]*Center for Complexity and Biosystems, Department of Physics "Aldo Pontremoli", University of Milan, Milano, Italy*

(Received 5 November 2025; revised 21 January 2026; accepted 23 January 2026; published 17 February 2026)

Predicting the failure and plasticity of solids remains a longstanding challenge, with broad implications for materials design and functional reliability. Disordered solids like metallic glasses can fail either abruptly or gradually without clear precursors, and the mechanical response depends strongly on composition, thermal history, and deformation protocol—impeding generalizable modeling. While deep learning methods offer predictive power, they often rely on numerous input parameters, hindering interpretability, methodology advancement, and practical deployment. We address this longstanding challenge with a macroscopic, physically grounded approach that uses plastic strain accumulation in the elastic regime to robustly predict deformation and yield. This method reduces complexity and improves interpretability, offering a practical alternative for disordered materials. For the Cu-Zr-(Al) metallic glasses prepared with varied annealing, we identify two limiting regimes of plastic strain growth: power law in poorly annealed and exponential in well-annealed samples. A physics-informed framework with Bayesian inference extracts growth parameters from stress-strain data within ∼5% strain, enabling early prediction of bulk response and yield point, well before the failure. The predictive performance improves with annealing and bulk plasticity correlates with the microscopic plastic activity from scattered to growth near yielding. This work presents a physically interpretable and experimentally relevant framework for predicting plasticity, stress-strain curve, and failure in metallic glasses from early mechanical response, offering both theoretical insights and practical tools for material characterization and design.

DOI: 10.1103/xf5s-kdyv

I. INTRODUCTION

Mechanical response in solids progresses from an initial elastic regime to plastic deformation, culminating in yielding and structural failure [1]. Predicting plastic response—identifying micro/macroscopic precursors and determining failure to be gradual (ductile) or abrupt (brittle)—remains a central challenge in materials science and engineering [2–4]. In crystalline solids, prediction of mechanical response is partially addressed by the framework of crystal plasticity [5,6], though the complete nature of defect dynamics and interactions remains elusive [7–13]. Amorphous materials—such as metallic glasses, molecular, and colloidal systems—represent the extreme limit of structural disorder. Unlike crystals, disordered solids lack apparent structural precursors—compounded by sensitivity to sample preparation and loading protocols [14–18], which makes predicting mechanical response and failure extremely challenging [19]. Overcoming these obstacles would enable accurate predictions of yielding and plastic flow in disordered systems, with significant implications for both fundamental understanding and practical applications.

Macroscale plasticity arises from localized shear events in shear transformation zones (STZs) [20–22], which are influenced by atomic-scale heterogeneity. Computational simulations have qualitatively examined various structural features—such as locally favored packings [23,24], compactness [25], local yield stress and shear modulus [26,27], soft vibrational modes [28–32]—all of which affect how plasticity emerges under deformation [33]. In crystalline solids again, this emergence is intimately coupled to how the topological defects, dislocations, respond to stress including dislocation multiplication mechanisms. In glasses, recent work has addressed this by constructing Burgers-vector-like quantities [34–37] and vertex-like quantities to measure the underlying topological order [38,39]. The hope is that as with dislocations a working definition of a structural defect indicates where STZs happen and would even allow one to predict the "failure" or shear-band formation where appropriate.

Modern machine learning (ML) methods [40] offer a promising pathway to uncover complex structural signatures that are otherwise obscure. Recent studies have proposed various ML techniques—including support vector machines (SVMs) [41], graph neural networks (GNNs) [42], unsupervised learning [43,44]—as well as elastoplastic models [45,46] to efficiently reveal underlying structure-property relationships. In the context of structure-mechanical response, ML and deep learning approaches have been used to build predictive frameworks—for example, convolutional neural networks (CNNs) to predict local plastic rearrangements [47], physics-informed networks to infer atomic structure [48], neural networks for prediction and nature of failure [49,50], and

*Contact author: tero.j.makinen@aalto.fi

†Contact author: anshul.parmar@ncbj.gov.pl

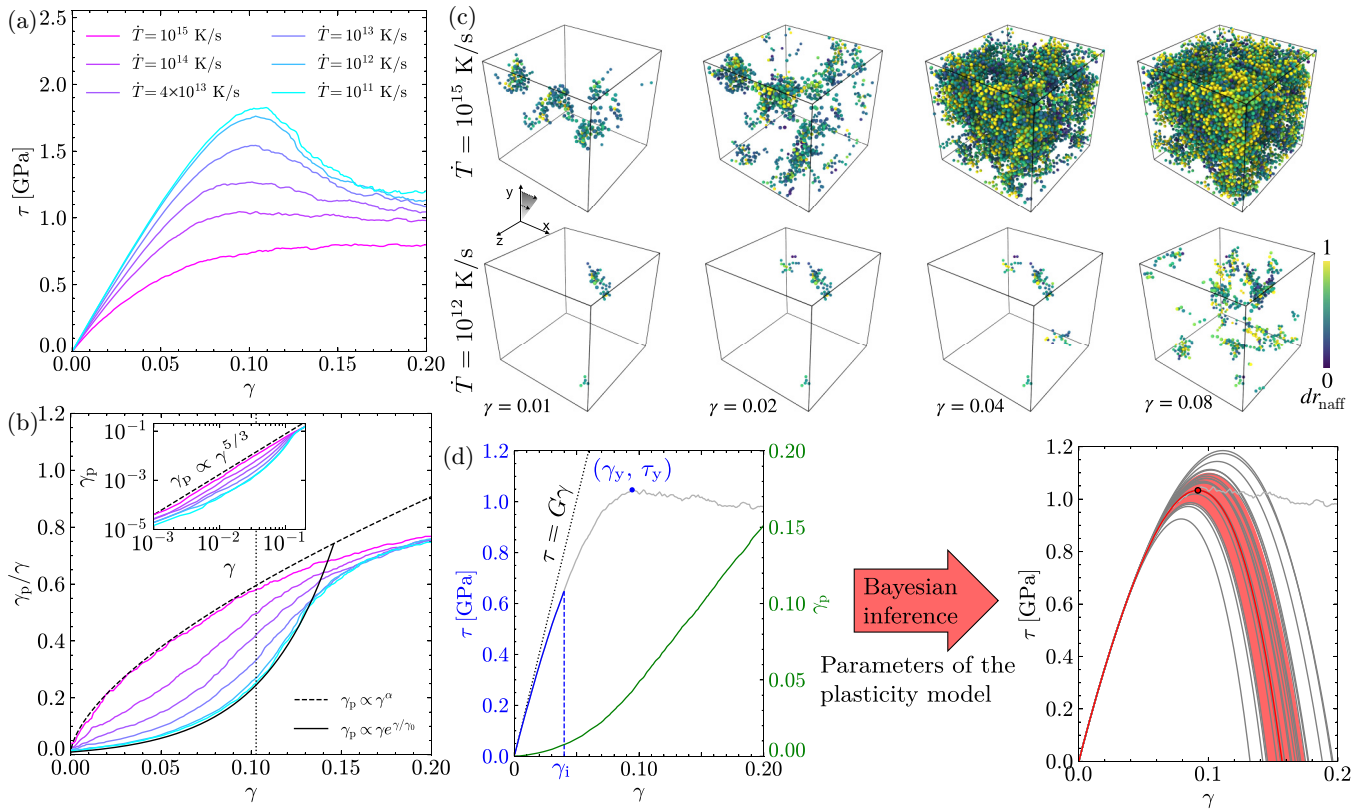

FIG. 1. (a) Stress-strain curves for glasses prepared with different cooling rates $\dot{T}$. (b) The proportion of plastic strain γ_p as a function of strain γ for each cooling rate [colors as in panel (a)]. The dashed and solid black lines are fits (up to $\gamma = 0.10$) to $\gamma_p \propto \gamma^{\alpha}$ and $\gamma_p \propto \gamma e^{\gamma/\gamma_0}$ for the extreme cooling rate cases, vertically shifted by 0.01 for clarity. The vertical dotted line corresponds to the average yield strain. The inset shows the plastic strain in a log-log plot, along with a power-law behavior (black dashed line). (c) The particles are colored by the nonaffine displacement dr_{naff} under a stress-drop, shown cumulatively for two cooling rates (rows) and four different global strains below the yield (columns). (d) The Bayesian prediction scheme: by reading the stress-strain curve up to a strain γ_i (blue part) we predict the yield point $(\gamma_y,\ \tau_y)$. This is done based on the accumulated plastic strain γ_p (green), which is determined from the difference to the perfect elastic behavior (black dashed line). We then infer the parameter distributions for the plasticity model, generate samples (each corresponding to a stress strain curve shown in gray), and finally average them to get the prediction (red line) and uncertainty estimates (light red shaded area). From the prediction we can get the yield point (red point).

GNN-based representations of microstructural deformation [51,52]. As defect evolution and interaction depend strongly on sample preparation and deformation protocols [14,15], no universal structural signature currently exists for predicting plasticity and catastrophic failure [33]. While deep learning effectively identifies structural defects and affinity with plastic events, its predictions—especially concerning macroscopic yield—often lack interpretability and physical insight.

In this work, we introduce a robust Bayesian machine learning framework to predict yielding in metallic glasses using macroscopic plasticity features. By focusing on plastic strain accumulation within the elastic regime—a physically meaningful and experimentally accessible indicator—we achieve accurate prediction of the entire curve as well as the yield stress and strain (see Fig. 1), something that, to our knowledge, has not been accomplished in either dislocation-mediated crystals or glassy systems. This macroscopic signal correlates with local rearrangements, such as STZs, underscoring its physical relevance. We demonstrate the broad applicability of the framework across ductile materials and preparation conditions, without requiring detailed microstructural, compositional, or thermal history inputs—making it both practical and interpretable. A number of recent studies have shown that early structural or vibrational signatures (such as machine-learned local structural indicators or low-frequency quasilocalized vibrational modes [53–55]) can also encode predictive information about subsequent dynamics and mechanical response in glasses. In this respect, the present approach is conceptually related to recent elastic-precursor and relaxation-based methods that exploit information encoded in the elastic regime to anticipate plastic events, although our focus is on macroscopic plastic strain accumulation under monotonic loading rather than configurational or relaxation metrics [56,57].

II. METHODS

A. System

In this study, we investigate the mechanical response of metallic glasses *in silico* using the binary $Cu_{0.50}Zr_{0.50}$ (as described in Ref. [58]) and a wide range of ternary Cu-Zr-Al amorphous compositions [59], shown in the Supplemental Material (SM) [60]. Molecular dynamics (MD) simulations are performed using LAMMPS [61], with atomic interactions

described by an embedded atom method (EAM) interatomic potential [62]. Simulations are primarily conducted on a system of 6000 atoms contained in a cubic box with periodic boundary conditions. To evaluate system size effects (see SM [60] for a discussion on these), larger systems comprising up to $N = 24000$ atoms are also simulated.

B. Sample preparation

Glass preparation is performed using a hybrid molecular dynamics–Monte Carlo (MD + MC) scheme within the variance-constrained semigrand canonical (VC-SGC) ensemble [63]. Rather than swapping atom types between a pair of particles, the method randomly selects a single atom and attempts to change its type. The acceptance of this trial move follows the Metropolis criterion, ensuring detailed balance while maintaining the target composition and efficient sampling of configurational space. To minimize compositional deviations, the parameters for chemical potential to perform the hybrid MD + MC simulations under the VC-SGC ensemble are provided by Ref. [64]. A similar hybrid scheme has also previously been applied to Cu-Zr systems [65].

The quenching is performed starting from molten metals at a high temperature well above the melting point using a fixed cooling rate $\dot{T}$ at fixed pressure $P = 0$ bar [64]. Six different cooling rates, ranging from 10^{11} to 10^{15} K/s, are employed to generate glasses with varying degrees of annealing, form well to poorly annealed states. In the MD + MC scheme a MC cycle consisting of N attempts is performed every 20 MD steps. The independent liquid samples are cooled from 2000 K to 300 K, with cooling rates ranging from 10^{11} to 10^{15}, ensuring an extended range of supercooled states [58].

C. Mechanical deformation

We perform athermal quasistatic shear (AQS) simulations under Lees-Edwards periodic boundary conditions. The simulation cell is incrementally sheared in the xy plane with a strain step of $\delta\gamma = 5 \times 10^{-6}$, followed by energy minimization using the conjugate gradient method. This protocol mimics the experimentally relevant conditions of low temperature and low shear rate, enabling a consistent stress-strain response for mechanical characterization. To obtain more experimental-representative stress-strain responses, we average the individual curves over 100 independent realizations of the disordered structure (50 for the slowest cooling rate). This statistical averaging approximates the response of a macroscopic sample composed of many representative volume elements. For optimized computation and structural analysis in the $N = 24000$ systems, we deformed the system using strain increments of $\delta\gamma = 10^{-4}$. To improve statistical averaging of avalanches, shear was applied independently along the xy, yz, and zx planes, since the system is isotropic.

We emphasize that the use of AQS is intended to isolate the structural-mechanical origins of plasticity. In contrast, deformation of metallic glasses under laboratory conditions at or slightly below the glass transition is generally activated and involves cooperative relaxation processes, such as string-like motions [66].

To quantify the mechanical response, we focus on the shear modulus (G) and the yield stress (τ_y). The shear modulus is determined from the stress-strain curves by averaging the positive slopes for the first 0.5% of strain in each of the independent realizations of the atomic configurations. The yield stress is determined from the average stress-strain curve over all the realizations and defined as the maximum shear stress attained during deformation.

D. Bayesian inference

The MCMC sampling from the posterior distribution [Eq. (4)] is done using PYMC [67] software and the No-U-Turn sampler (NUTS) [68]. We run four chains in parallel and for each discard the first 1000 tuning samples, after which we record 2000 samples. The full model is

$$\tau = G(\gamma - A\gamma^{\alpha} e^{\gamma/\gamma_0}) + \epsilon, \tag{1}$$

where G is the constant shear modulus (see SM [60] for discussion on the constancy of the modulus) and ϵ is the noise observed. The noise is implemented through the use of a Gaussian likelihood on the logarithm of the stress

$$p(\mathcal{D}|\theta) = \prod_k \frac{\exp\left(-\frac{(\ln\tau_k - \ln[G(\gamma_k - A\gamma_k^{\alpha} e^{\frac{\gamma_k}{\gamma_0}})])^2}{2\sigma_\epsilon^2}\right)}{\sqrt{2\pi\sigma_\epsilon^2}}, \tag{2}$$

where the index k runs through all the data points in $\mathcal{D}$. The logarithm is there to give more focus to the early part of the stress-strain curves, where the stress is low. We have used a half-normal prior for σ_ϵ with a standard deviation of 0.1 GPa. Based on the knowledge of the valid range for the exponent α, we use an informative prior, namely the uniform distribution between 1 and 2. For the parameters A and γ_0 we use weakly informative log-normal priors, with the probability density function $p(x) \propto \exp[-(\ln x - \mu)^2/(2\sigma^2)]$, and the values $[\mu = \ln(0.2), \sigma = 4]$ for both A and γ_0.

Each sample of A, α, and γ_0 can then be used to generate the evolution of the plastic strain using Eq. (3) and the full stress-strain curve using $\tau = G(\gamma - \gamma_p)$. The yield point is then determined from the condition $\partial\gamma_p/\partial\gamma = 1$ for each of these curves. This yields a distribution of stresses for each strain value, as well as distributions for the yield stress τ_y and the yield strain γ_y.

E. Microscopic estimates of plasticity

During an avalanche, the system can be viewed microscopically as comprising a core region of plastically deformed particles, while the surrounding material undergoes elastic deformation in response to the stress induced by the applied strain. A particle is classified as "plastic" if its displacement exceeds 0.30 Å. This displacement threshold is chosen to include particles actively involved in plastic deformation while excluding those responding elastically. It is identical to the criterion used in our previous study [58], where it was shown to correspond to the onset of the nonaffine displacement tail associated with shear transformation events. More generally, this definition is consistent with mobile-immobile particle partitioning schemes commonly used to identify dynamic heterogeneities in glasses [69].

The fraction of particles participating in the plastic response during an avalanche is quantified as $n_p = N_p/N$, where N_p is the number of plastically displaced particles and N is the total number of particles. To perform a comparative study with the bulk plastic strain, we also observe the particles cumulatively ($n_{c,p}$) over a range of strain values. Additionally, a pair of such particles is considered part of the same "cluster" if they lie within the first coordination shell, as defined by the pair correlation function [$g(r)$]. A cluster is considered percolating if it spans the entire system and its size scales with the system size.

III. RESULTS

A. Mechanical response

We obtain the mechanical response of the samples by shearing them using the AQS protocol across the yielding strain and record the stress-strain response [see Fig. 1(a)]. Depending on the cooling rate $\dot{T}$ used for glass preparation, we observe strongly varying behavior. For slow cooling rates, we observe a long linear—close to elastic—behavior extending to around $\gamma = 5\%$. For faster cooling rates, the initial slope of the stress-strain curves, i.e., shear moduli G, is lower, and the variation from linear behavior starts almost immediately. Additionally, slower cooling rates result in higher peak stresses, with a more pronounced maximum in the stress-strain curves. We define the maximum shear stress as the yield stress τ_y and the corresponding strain as the yield strain γ_y. This working definition may be ambiguous for poorly annealed glasses, where the maximum stress can occur within the steady-state flow regime. Nevertheless, we adopt this single definition of yield to ensure consistent comparison across glasses prepared with different annealing (see SM [60] for an alternative yield strain definition).

The initial modulus G allows for the determination of the plastic strain using the relation $\gamma_p = \gamma - \frac{\tau}{G}$ (see SM [60] for discussion on the constancy of G). Looking at the evolution of this quantity [illustrated in Fig. 1(b)], we observe two extreme cases: a power law $\gamma_p \propto \gamma^\alpha$ for fast cooling rates and a mix of linear and exponential behavior $\gamma_p \propto \gamma e^{\gamma/\gamma_0}$ for the slow cooling rates. The latter is essentially exponential behavior, with a linear part at low strains $\gamma \ll \gamma_0$—giving the correct $\gamma_p \to 0$ behavior at the $\gamma \to 0$ limit.

Figure 1(c) provides a microscopic visualization of the accumulated plastic strain in glasses annealed at cooling rates $\dot{T} = 10^{15}$ (top) and $\dot{T} = 10^{12}$ (bottom), for systems with $N = 24000$ particles. Particles rearranged in a plastic event are highlighted based on a nonaffine displacement threshold of $dr_{\text{naff.}} > 0.3$ Å (see Materials and Methods and Ref. [58]). These highlighted particles, identified during individual plastic events and shown cumulatively over a range of strain values, represent the evolving spatial profile of local plastic activity, which can be considered representative of shear transformation zones or softness [33].

Plastic activity appears spatially extensive in the poorly annealed glass, whereas in the well-annealed glass it remains more localized. This localization, understood to be correlated with the spatial distribution of soft regions, is also observed in the local yield stress and elastic moduli [26,27,33]. As yielding approaches, we observe that these initially isolated soft regions grow, leading to relative growth of the clusters of plastically deformed particles—consistent with the observed growth behavior of the global plastic strain.

B. Bayesian prediction model

To predict the yielding behavior of the glasses we construct a function that can encompass both of the extreme cases and interpolate between them, namely

$$\gamma_p = A\gamma^\alpha e^{\gamma/\gamma_0}, \tag{3}$$

where we explictly introduce the prefactor A. This reproduces the slow cooling rate near-exponential behavior with $\alpha = 1$, and in the $\gamma_0 \to \infty$ limit depicts the pure power-law behavior, as observed for the faster cooling. Using this function, we can make early predictions of the yield point (γ_y, τ_y), based on the stress-strain data read only up to a low strain value γ_i. The goal is to infer the values of the parameter set $\theta = \{A, \gamma_0, \alpha\}$ based on the observed data $\mathcal{D}$ (stress-strain data up to strain γ_i) and to extrapolate the stress-strain behavior at future strains from $\tau = G(\gamma - \gamma_p)$. This process is shown in Fig. 1(d).

We do prediction using Bayesian inference, which starts from the Bayes' theorem

$$p(\theta|\mathcal{D}) = \frac{p(\mathcal{D}|\theta)p(\theta)}{p(\mathcal{D})} = \frac{p(\mathcal{D}|\theta)p(\theta)}{\int p(\mathcal{D}|\theta)p(\theta)\mathrm{d}\theta}, \tag{4}$$

where $p(\theta|\mathcal{D})$ is the posterior distribution of the parameters conditional on the observed data, $p(\mathcal{D}|\theta)$ the likelihood, and $p(\theta)$ the prior distribution encoding our knowledge about the parameters before observing any data. The integral over all the possible parameter values in the marginal likelihood $p(\mathcal{D})$ is generally analytically intractable, but Markov chain Monte Carlo (MCMC) methods can be used to generate a sequence of parameter values, the distribution of which approximates the posterior distribution. Compared to simple curve fitting, Bayesian inference provides both regularization through priors and robust uncertainty quantification, which is used to assess the reliability of predictions and the convergence of the ML algorithm. Here we read the stress-strain data (γ, τ) up to a strain γ_i and use this as the observed data $\mathcal{D}$. Using MCMC we then sample from the posterior distribution [Eq. (4)], and for each sample can compute the plastic strain [Eq. (3)], generate a stress-strain curve, and finally determine the corresponding yield point (γ_y, τ_y). See Materials and Methods section for more details on the implementation.

Taking as an example the prediction strain of $\gamma_i = 5\%$ shows the power of the proposed framework [see Fig. 2(a)]. By only considering small strains, in the near-linear elastic regime, we still observe enough plasticity to be able to infer fairly narrow distributions for the model parameters θ, thus having fairly narrow distributions for the predictions of yield stress τ_y and strain γ_y. For the slower cooling rates the prediction is excellent, closely following the shape of the stress-strain curves up to yielding. For poorly annealed glasses, where the yield point is ill-defined and plastic strain accumulates slower than predicted, the model tends to underestimate the yield stress by around 20%. Nevertheless, the predictions remain reasonably accurate and relevant for practical engineering applications (see SM [60] for further

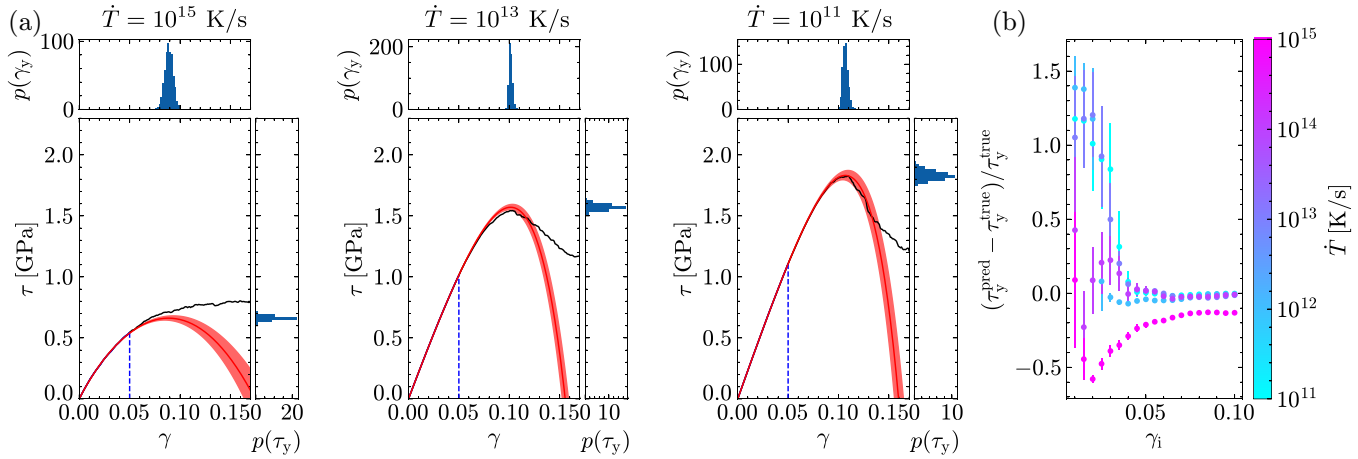

FIG. 2. (a) Bayesian prediction of the stress-strain curve for three different cooling rates $\dot{T}$. The red curve is the average stress-strain prediction (shaded area corresponding to the uncertainty estimate), made based on the data before $\gamma_i = 5\%$ (blue dashed line). The probability distributions of the yield stress $p(\tau_y)$ and yield strain $p(\gamma_y)$ derived from the individual prediction samples are shown on top and on the side of the figures. (b) The relative difference between the predicted τ_y^{pred} and true value τ_y^{true} of the yield stress as a function of the prediction strain γ_i for the different cooling rates. Although the yield stress is ill-defined in poorly annealed glasses, the predictions remain sufficiently accurate (with ∼20% underestimation of stress).

discussion). The prediction accuracy naturally increases, as one takes more data into account (i.e., increases γ_i) and the predictions start to converge to the correct values at around $\gamma_i = 5\%$ [see Fig. 2(b)]. See SM [60] for more discussion on the posterior distributions of the parameters (including the connection between A and γ_0), as well as the posterior distributions of τ_y and γ_y, with changing γ_i.

C. Two limiting behaviors

The inferred posterior distributions of the parameters of α and γ_0 of Eq. (3) are very narrow (see error bars in Fig. 3). We can also see that the posterior distributions do not evolve much going from strain $\gamma_i = 0.05$ to $\gamma_i = 0.08$ (see difference

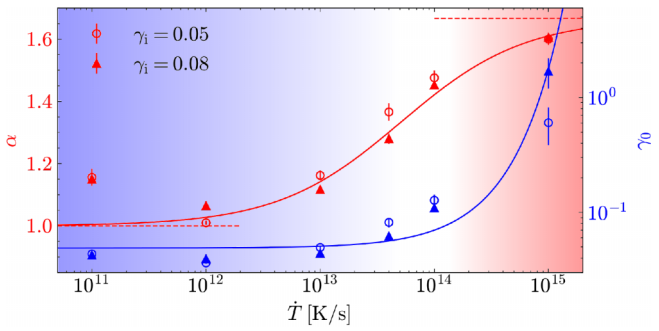

FIG. 3. Mean behavior of the inferred values of the parameters of Eq. (3) for α (red) and γ_0 (blue) for each cooling rate and for two different Bayesian prediction strains γ_i. The dashed red lines correspond to the linear ($\alpha = 1$) and percolation cluster ($\alpha = 5/3$) behaviors and the solid red line a logistic fit going from one limiting behavior into the other. The solid blue line corresponds to an exponential fit. The background color indicates the cooling rates dominated by the exponential behavior (blue) and the ones dominated by the power-law behavior (red). Both the fits and color gradient serve as guides to the eye.

of open circles and filled triangles in Fig. 3). One can also see the expected behavior for the extreme cases: for slow cooling rates γ_0 is low, indicating exponential behavior with the low strain power-law regime having close to linear behavior ($\alpha \approx 1$) and for high cooling rates γ_0 is very high, indicating dominant power-law behavior. This is qualitatively shown in the background color of Fig. 3. Such power-law and exponential behaviors have previously been seen also in dislocation plasticity [11].

We next outline an argument for the development of plasticity in "bad" glasses where the γ_p exhibits a power-law-like growth. With the observation that the number of atoms participating in yielding scales as $n \simeq \gamma^\alpha$, we write the growth law for n as

$$\frac{\partial n}{\partial \gamma} \simeq n^{(\alpha-1)/\alpha}. \tag{5}$$

We next assume that the growth takes place in diffuse clusters of internal dimension d_f and a surface dimension d_s for n and cluster size S as a function of the cluster linear dimension R. If the growth rate Δn is taken proportional to S, we solve α and obtain that

$$\alpha = \frac{d_f}{d_f - d_s}. \tag{6}$$

For 3D isotropic percolation these exponents have the values $d_f \simeq 2.53$ and $d_s \simeq 1.03$ which gives with quite a good approximation $\alpha = 5/3$. This matches the limiting behavior we see at high $\dot{T}$ (Fig. 3). The microscopic observations for the poorly annealed glass are also consistent with the fractal dimension of 3D isotropic percolation, which is observed well beyond the yield point and transient shear band (see SM [60]). These limits should be "universal" in bounding the plasticity development, thus the shape of the stress-strain curve, and lead to the demonstration in the SM [60] how various compositions of the CuZrAl family at a fixed cooling rate map into CuZr with different cooling rates.

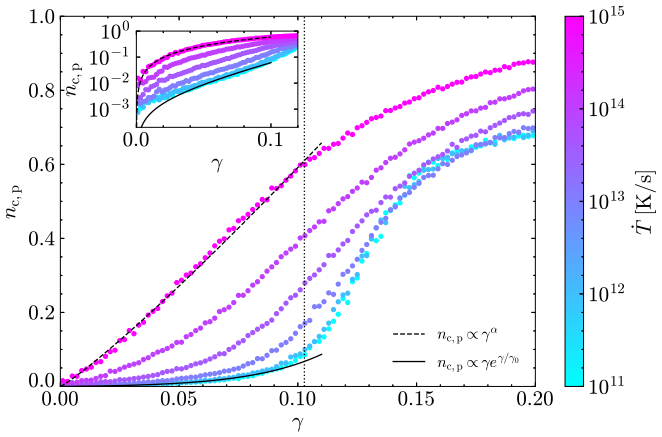

FIG. 4. Cumulative fraction of yielded particles $n_{c,p}$ as a function of the applied strain γ for the different cooling rates. The inset shows the same data in a logarithmic-linear plot to illustrate the exponential behavior in the plasticity in the preyield regime. The vertical dashed line marks the averaged yielding strain for all the cooling rates.

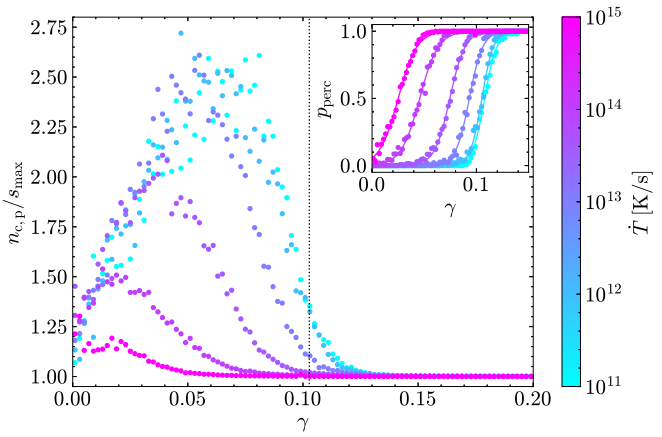

FIG. 5. Ratio between the cumulative fraction of yielded particles $n_{c,p}$ and the size of maximum cluster s_{max} as a function of the applied strain γ for the different cooling rates. In the preyield regime, the systematic increase in the peak of the $n_{c,p}/s_{max}$ suggests that plastic events are distinct till the strain $\gamma \sim 0.05$, which further percolates to form the spanning cluster. The inset shows the percolation probability p_{perc} and a logistic fit. The vertical dashed line marks the averaged yielding strain for all the cooling rates.

D. Microscopic nature of plasticity

To gain microscopic insights with a structural perspective, we examine the fraction of particles (n_p) involved in irreversible plastic deformation. During an avalanche, a particle is considered part of the plastic core if its nonaffine displacement exceeds 0.3 Å. This displacement threshold allows the identification of particles undergoing plastic rearrangements at the microscopic level (see Materials and Methods for details and Refs. [14,58]). Recognizing such particles serves as a tool for identifying local rearrangments (STZs), the fundamental units of plastic deformation. The particles involved in an avalanche exhibit a physically consistent correlation with the active participation in the bulk stress drops (as discussed in SM [60] and Ref. [58]), further asserting the physical relevance of this observation.

To track the development of plasticity, we monitor these particle fractions cumulatively ($n_{c,p}$)—from the initial undeformed state to well beyond the yield strain. Figure 4 shows the cumulative fraction of particles exhibiting plastic activity for various cooling rates. In the nearly elastic regime, the poorly annealed glass exhibits weak power-law behavior with an exponent of $\alpha = 1.12$. The observed exponent is noticeably smaller than that for bulk plastic strain, possibly due to the absence of long-range elastoplastic responses in the present microscopic analysis, which are inherently difficult to distinguish from local effects [14]. As the degree of annealing increases, the evolution of plasticity gradually transitions toward an exponential form. This cumulative microscopic evolution resembles the behavior of the macroscopic plastic strain, highlighting a consistent correlation between atomistic dynamics and bulk mechanical response.

E. Microscopic signal for machine learning predictability

To further explore the development of bulk plasticity under shear, we perform a spatial analysis based on the cumulative clustering of particles undergoing plastic rearrangements. Two particles are considered part of the same cluster if they are neighbors, defined as being within the first coordination shell according to the radial distribution function. Similar to the cumulative fraction of yielded particles ($n_{c,p}$) and bulk plastic strain, the size of the largest cluster also increases and exhibits a comparable dependence on the cooling rate (see SM [60]).

To highlight the spatial nature of plasticity, Fig. 5 shows the ratio of the cumulative fraction of particles undergoing plastic rearrangements, $n_{c,p}$, to the size of the largest cluster, s_{max}, as a function of strain γ across cooling rates. As noted in Fig. 1, plastic activity is spatially extensive in poorly annealed glasses, forming percolating clusters early in deformation. In contrast, plasticity in better-annealed glasses is more localized: the ratio gradually increases and peaks, which depends on the cooling rate, indicating that plastic events remain spatially distinct within the initial-elastic limit (up to 5% strain). Beyond this point, as observed, events begin to merge into a spanning cluster and grow. However, full percolation requires additional loading and further distinct plastic events. These findings demonstrate that the spatial distribution and growth of plasticity, even in the near-elastic regime, encode structurally relevant information, observed to be effectively captured by our ML-based model and motivating its extension to brittle glasses to test broader applicability.

IV. CONCLUSIONS

This work presents a predictive framework for the mechanical response of Cu-Zr(-Al) metallic glasses under shear, combining physical insight with Bayesian machine learning. By analyzing plastic strain evolution in the early elastic regime, we show that stress-strain curve and yield point can be accurately predicted across a broad range of cooling rates associated with ductile failure. Plasticity develops progressively and reflects the thermal history of the glass, with preyield activity more localized in well-annealed samples and more

extensive in poorly annealed ones. Bulk plastic strain, associated with the plastic rearrangements, emerges as a key predictive feature.

Our approach replaces the complexity of multivariable models into a small set of physically meaningful, global observables, e.g., stress and plastic strain, without relying on detailed microscopic inputs that are often specific to a given system or thermal history [33]. It is computationally efficient, broadly applicable across different preparation conditions, compositions (see SM [60]), and physically interpretable. Importantly, our method overcomes key limitations of commonly used deep learning approaches, offering a more transparent, transferable framework. While demonstrated under athermal quasistatic shear conditions, extending this work to finite temperatures and shear rates (where thermally activated relaxation and rate-dependent plasticity become important), as well as to ductile-to-brittle transitions offers a promising direction for future work [15,70]. This would require incorporating additional physical ingredients beyond early plastic strain accumulation. Our findings encourage a deeper exploration of plasticity growth with multiscale modeling and its connection to yielding through theoretical studies, atomistic simulations, and mesoscale elastoplastic models. This study shows that physics-informed machine learning with bulk plasticity can provide robust, interpretable, and transferable predictions of yielding in disordered materials, directly relevant to experiments and applications.

The present framework assumes that plastic strain accumulates progressively in the nominally elastic regime, allowing a smooth growth law inferred at small strains to be extrapolated toward yielding. This assumption is well justified for ductile and marginally stable glasses, but it breaks down for sufficiently well-annealed glasses that exhibit brittle, discontinuous yielding associated with a spinodal-like instability near the yield point [15]. In such cases, plastic activity does not evolve as a smooth continuation of early plasticity and the present extrapolation strategy is not expected to remain valid. Extending the framework to brittle glasses would require incorporating additional indicators of proximity to yielding, such as spinodal-like signatures or changes in collective plastic activity, which remains an interesting direction for future work.

ACKNOWLEDGMENTS

A.D.S.P., S.B., and M.J.A. are supported by the European Union Horizon 2020 Research and Innovation Program under Grant Agreement No. 857470 and from the European Regional Development Fund via the Foundation for Polish Science International Research Agenda PLUS program Grant No. MAB PLUS/2018/8. M.J.A. acknowledges support from the Academy of Finland (Grants No. 361245 and No. 317464) and from the Finnish Cultural Foundation. S.B. acknowledges support from the National Science Center in Poland through the SONATA BIS Grant No. DEC-2023/50/E/ST3/00569 and from the Foundation for Polish Science in Poland through the FIRST TEAM Project No. FENG.02.02-IP.05-0177/23 project. T.M. and M.J.A. acknowledge support from the FinnCERES flagship (Grant No. 151830423), Business Finland (Grants No. 211835, No. 211909, and No. 211989), the Research Council of Finland (Grant No. 13361245), and Future Makers programs. The authors acknowledge the computational resources provided by the Aalto University School of Science "Science-IT" project.

T.M. and A.D.S.P. contributed equally in the work; T.M., A.D.S.P., and M.J.A. designed the research; T.M. and A.D.S.P. performed the simulations; T.M., A.D.S.P., S.B., and M.J.A. analyzed the data and wrote the paper.

DATA AVAILABILITY

The data that support the findings of this article are openly available [71].

[1] L. Berthier, G. Biroli, L. Manning, and F. Zamponi, Yielding and plasticity in amorphous solids, Nat. Rev. Phys. **7**, 313 (2025).

[2] R. von Mises, Mechanik der festen Körper im plastisch-deformablen Zustand, Nachr. Ges. Wiss. Goettingen, Math.-Phys. Kl. **4**, 582 (1913).

[3] R. Hill, A theory of the yielding and plastic flow of anisotropic metals, Proc. R. Soc. Lond. A **193**, 281 (1948).

[4] T. Divoux, E. Agoritsas, S. Aime, C. Barentin, J.-L. Barrat, R. Benzi, L. Berthier, D. Bi, G. Biroli, D. Bonn, *et al.*, Ductile-to-brittle transition and yielding in soft amorphous materials: Perspectives and open questions, Soft Matter **20**, 6868 (2024).

[5] N. Aravas and E. Aifantis, On the geometry of slip and spin in finite plastic deformation, Int. J. Plast. **7**, 141 (1991).

[6] L. Anand and M. Kothari, A computational procedure for rate-independent crystal plasticity, J. Mech. Phys. Solids **44**, 525 (1996).

[7] R. E. Miller and D. Rodney, On the nonlocal nature of dislocation nucleation during nanoindentation, J. Mech. Phys. Solids **56**, 1203 (2008).

[8] M.-C. Miguel, A. Vespignani, S. Zapperi, J. Weiss, and J.-R. Grasso, Intermittent dislocation flow in viscoplastic deformation, Nature (London) **410**, 667 (2001).

[9] H. Salmenjoki, A. Lehtinen, L. Laurson, and M. J. Alava, Plastic yielding and deformation bursts in the presence of disorder from coherent precipitates, Phys. Rev. Mater. **4**, 083602 (2020).

[10] K. A. Dahmen, Y. Ben-Zion, and J. T. Uhl, Micromechanical model for deformation in solids with universal predictions for stress-strain curves and slip avalanches, Phys. Rev. Lett. **102**, 175501 (2009).

[11] P. D. Ispánovity, I. Groma, G. Györgyi, F. F. Csikor, and D. Weygand, Submicron plasticity: Yield stress, dislocation avalanches, and velocity distribution, Phys. Rev. Lett. **105**, 085503 (2010).

[12] P. D. Ispánovity, L. Laurson, M. Zaiser, I. Groma, S. Zapperi, and M. J. Alava, Avalanches in 2D dislocation systems: Plastic yielding is not depinning, Phys. Rev. Lett. **112**, 235501 (2014).

[13] H. Salmenjoki, M. J. Alava, and L. Laurson, Machine learning plastic deformation of crystals, Nat. Commun. **9**, 5307 (2018).

[14] P. Leishangthem, A. D. Parmar, and S. Sastry, The yielding transition in amorphous solids under oscillatory shear deformation, Nat. Commun. **8**, 14653 (2017).
[15] M. Ozawa, L. Berthier, G. Biroli, A. Rosso, and G. Tarjus, Random critical point separates brittle and ductile yielding transitions in amorphous materials, Proc. Natl. Acad. Sci. USA **115**, 6656 (2018).
[16] A. D. S. Parmar, S. Kumar, and S. Sastry, Strain localization above the yielding point in cyclically deformed glasses, Phys. Rev. X **9**, 021018 (2019).
[17] H. Bhaumik, G. Foffi, and S. Sastry, The role of annealing in determining the yielding behavior of glasses under cyclic shear deformation, Proc. Natl. Acad. Sci. USA **118**, e2100227118 (2021).
[18] W.-T. Yeh, M. Ozawa, K. Miyazaki, T. Kawasaki, and L. Berthier, Glass stability changes the nature of yielding under oscillatory shear, Phys. Rev. Lett. **124**, 225502 (2020).
[19] F. Spaepen, A microscopic mechanism for steady state inhomogeneous flow in metallic glasses, Acta Metall. **25**, 407 (1977).
[20] A. Argon, Plastic deformation in metallic glasses, Acta Metall. **27**, 47 (1979).
[21] M. L. Falk and J. S. Langer, Dynamics of viscoplastic deformation in amorphous solids, Phys. Rev. E **57**, 7192 (1998).
[22] A. Nicolas, E. E. Ferrero, K. Martens, and J.-L. Barrat, Deformation and flow of amorphous solids: Insights from elastoplastic models, Rev. Mod. Phys. **90**, 045006 (2018).
[23] D. Coslovich and G. Pastore, Understanding fragility in supercooled Lennard-Jones mixtures. I. Locally preferred structures, J. Chem. Phys. **127**, 124504 (2007).
[24] J. Paret, R. L. Jack, and D. Coslovich, Assessing the structural heterogeneity of supercooled liquids through community inference, J. Chem. Phys. **152**, 144502 (2020).
[25] H. Tong and H. Tanaka, Revealing hidden structural order controlling both fast and slow glassy dynamics in supercooled liquids, Phys. Rev. X **8**, 011041 (2018).
[26] M. Tsamados, A. Tanguy, C. Goldenberg, and J.-L. Barrat, Local elasticity map and plasticity in a model Lennard-Jones glass, Phys. Rev. E **80**, 026112 (2009).
[27] S. Patinet, D. Vandembroucq, and M. L. Falk, Connecting local yield stresses with plastic activity in amorphous solids, Phys. Rev. Lett. **117**, 045501 (2016).
[28] A. Widmer-Cooper, H. Perry, P. Harrowell, and D. R. Reichman, Irreversible reorganization in a supercooled liquid originates from localized soft modes, Nat. Phys. **4**, 711 (2008).
[29] A. Tanguy, B. Mantisi, and M. Tsamados, Vibrational modes as a predictor for plasticity in a model glass, Europhys. Lett. **90**, 16004 (2010).
[30] M. L. Manning and A. J. Liu, Vibrational modes identify soft spots in a sheared disordered packing, Phys. Rev. Lett. **107**, 108302 (2011).
[31] L. Gartner and E. Lerner, Nonlinear plastic modes in disordered solids, Phys. Rev. E **93**, 011001(R) (2016).
[32] S. Bonfanti, R. Guerra, C. Mondal, I. Procaccia, and S. Zapperi, Elementary plastic events in amorphous silica, Phys. Rev. E **100**, 060602(R) (2019).
[33] D. Richard, M. Ozawa, S. Patinet, E. Stanifer, B. Shang, S. A. Ridout, B. Xu, G. Zhang, P. K. Morse, J.-L. Barrat, *et al.*, Predicting plasticity in disordered solids from structural indicators, Phys. Rev. Mater. **4**, 113609 (2020).
[34] A. Bera, I. Regev, A. Zaccone, and M. Baggioli, Burgers rings as topological signatures of Eshelby-like plastic events in glasses, arXiv:2505.23069.
[35] A. Bera, D. Majumdar, T. W. Sirk, I. Regev, and A. Zaccone, Microscopic origin of shear bands in 2D amorphous solids from topological defects, arXiv:2507.09250.
[36] A. C. Liu, H. Pham, A. Bera, T. C. Petersen, T. W. Sirk, S. T. Mudie, R. F. Tabor, J. Nunez-Iglesias, A. Zaccone, and M. Baggioli, Measurable geometric indicators of local plasticity in glasses, Acta Crystallogr. **A82**, 4 (2026).
[37] A. Bera, M. Baggioli, T. C. Petersen, T. W. Sirk, A. C. Liu, and A. Zaccone, Clustering of negative topological charges precedes plastic failure in 3D glasses, PNAS Nexus **3**, pgae315 (2024).
[38] Z. W. Wu, Y. Chen, W.-H. Wang, W. Kob, and L. Xu, Topology of vibrational modes predicts plastic events in glasses, Nat. Commun. **14**, 2955 (2023).
[39] Z. W. Wu, J.-L. Barrat, and W. Kob, On the geometry of topological defects in glasses, Nat. Commun. **17**, 217 (2026).
[40] G. Jung, R. M. Alkemade, V. Bapst, D. Coslovich, L. Filion, F. P. Landes, A. J. Liu, F. S. Pezzicoli, H. Shiba, G. Volpe, *et al.*, Roadmap on machine learning glassy dynamics, Nat. Rev. Phys. **7**, 91 (2025).
[41] S. S. Schoenholz, E. D. Cubuk, D. M. Sussman, E. Kaxiras, and A. J. Liu, A structural approach to relaxation in glassy liquids, Nat. Phys. **12**, 469 (2016).
[42] V. Bapst, T. Keck, A. Grabska-Barwińska, C. Donner, E. D. Cubuk, S. Schoenholz, A. Obika, A. Nelson, T. Back, D. Hassabis, *et al.*, Unveiling the predictive power of static structure in glassy systems, Nat. Phys. **16**, 448 (2020).
[43] E. Boattini, M. Dijkstra, and L. Filion, Unsupervised learning for local structure detection in colloidal systems, J. Chem. Phys. **151**, 154901 (2019).
[44] E. Boattini, S. Marín-Aguilar, S. Mitra, G. Foffi, F. Smallenburg, and L. Filion, Autonomously revealing hidden local structures in supercooled liquids, Nat. Commun. **11**, 5479 (2020).
[45] G. Zhang, S. A. Ridout, and A. J. Liu, Interplay of rearrangements, strain, and local structure during avalanche propagation, Phys. Rev. X **11**, 041019 (2021).
[46] B. Xu, Z. Wu, J. Lu, M. D. Shields, C. H. Rycroft, F. Bamer, and M. L. Falk, Stochastic evolution elasto-plastic modeling of a metallic glass, arXiv:2410.00760.
[47] Z. Fan and E. Ma, Predicting orientation-dependent plastic susceptibility from static structure in amorphous solids via deep learning, Nat. Commun. **12**, 1506 (2021).
[48] M. L. Bødker, M. Bauchy, T. Du, J. C. Mauro, and M. M. Smedskjaer, Predicting glass structure by physics-informed machine learning, npj Comput. Mater. **8**, 192 (2022).
[49] F. Font-Clos, M. Zanchi, S. Hiemer, S. Bonfanti, R. Guerra, M. Zaiser, and S. Zapperi, Predicting the failure of two-dimensional silica glasses, Nat. Commun. **13**, 2820 (2022).
[50] Z. Fan, E. Ma, and M. L. Falk, Predicting the location of shear band initiation in a metallic glass, Phys. Rev. Mater. **6**, 065602 (2022).
[51] A. Thomas, A. R. Durmaz, M. Alam, P. Gumbsch, H. Sack, and C. Eberl, Materials fatigue prediction using graph neural networks on microstructure representations, Sci. Rep. **13**, 12562 (2023).

[52] H. Zhai, Stress predictions in polycrystal plasticity using graph neural networks with subgraph training, Comput. Mech. **76**, 387 (2025).

[53] H. Shiba, M. Hanai, T. Suzumura, and T. Shimokawabe, BOTAN: BOnd TArgeting Network for prediction of slow glassy dynamics by machine learning relative motion, J. Chem. Phys. **158**, 084503 (2023).

[54] N. Oyama, S. Koyama, and T. Kawasaki, What do deep neural networks find in disordered structures of glasses? Front. Phys. **10**, 1007861 (2023).

[55] M. Liu, S. Koyama, N. Oyama, and H. Mizuno, Quasi-localized vibrations arise from liquid-like structures in glasses: Insights from deep neural networks, J. Appl. Phys. **138**, 044704 (2025).

[56] Z.-Y. Zhou, Q. Yang, and H.-B. Yu, Toward atomic-scale understanding of structure-dynamics-properties relations for metallic glasses, Prog. Mater. Sci. **145**, 101311 (2024).

[57] H.-B. Yu, L. Gao, J.-Q. Gao, and K. Samwer, Universal origin of glassy relaxation as recognized by configuration pattern matching, Natl. Sci. Rev. **11**, nwae091 (2024).

[58] T. Mäkinen, A. D. S. Parmar, S. Bonfanti, and M. J. Alava, Avalanches in Cu-Zr-Al metallic glasses, Phys. Rev. E **111**, 014107 (2025).

[59] T. Mäkinen, A. D. S. Parmar, S. Bonfanti, and M. J. Alava, Bayesian exploration of the composition space of CuZrAl metallic glasses for mechanical properties, npj Comput. Mater. **11**, 96 (2025).

[60] See Supplemental Material at https://link.aps.org/supplemental/10.1103/xf5s-kdyv for additional information on the extension to different compositions, system size effects, the alternative yield strain definition, evolution of the shear modulus, posterior distributions of the model parameters, the prefactor of the plasticity model, posterior distributions of the predicted quantities, and particle's irreversible rearrangement under deformation and the fractal dimension.

[61] A. P. Thompson, H. M. Aktulga, R. Berger, D. S. Bolintineanu, W. M. Brown, P. S. Crozier, P. J. in 't Veld, A. Kohlmeyer, S. G. Moore, T. D. Nguyen, R. Shan, M. J. Stevens, J. Tranchida, C. Trott, and S. J. Plimpton, LAMMPS—a flexible simulation tool for particle-based materials modeling at the atomic, meso, and continuum scales, Comp. Phys. Comm. **271**, 10817 (2022).

[62] Y. Q. Cheng, E. Ma, and H. W. Sheng, Atomic level structure in multicomponent bulk metallic glass, Phys. Rev. Lett. **102**, 245501 (2009).

[63] B. Sadigh, P. Erhart, A. Stukowski, A. Caro, E. Martinez, and L. Zepeda-Ruiz, Scalable parallel Monte Carlo algorithm for atomistic simulations of precipitation in alloys, Phys. Rev. B **85**, 184203 (2012).

[64] F. Kaskosz, R. Alvarez-Donado, M. Alava, A. D. S. Parmar, and S. Bonfanti, Efficient sampling method for multi-component ZrCu(Al) metallic glasses, arXiv:2309.05806.

[65] Z. Zhang, J. Ding, and E. Ma, Shear transformations in metallic glasses without excessive and predefinable defects, Proc. Natl. Acad. Sci. USA **119**, e2213941119 (2022).

[66] Q. Wang, L.-F. Zhang, Z.-Y. Zhou, and H.-B. Yu, Predicting the pathways of string-like motions in metallic glasses via path-featurizing graph neural networks, Sci. Adv. **10**, eadk2799 (2024).

[67] O. Abril-Pla, V. Andreani, C. Carroll, L. Dong, C. J. Fonnesbeck, M. Kochurov, R. Kumar, J. Lao, C. C. Luhmann, O. A. Martin, M. Osthege, R. Vieira, T. Wiecki, and R. Zinkov, PyMC: A modern, and comprehensive probabilistic programming framework in Python, PeerJ Comput. Sci. **9**, e1516 (2023).

[68] M. D. Hoffman and A. Gelman, The no-U-turn sampler: Adaptively setting path lengths in Hamiltonian Monte Carlo, J. Mach. Learn. Res. **15**, 1593 (2014).

[69] L. Gao, H.-B. Yu, T. B. Schrøder, and J. C. Dyre, Unified percolation scenario for the α and β processes in simple glass formers, Nat. Phys. **21**, 471 (2025).

[70] M. Singh, M. Ozawa, and L. Berthier, Brittle yielding of amorphous solids at finite shear rates, Phys. Rev. Mater. **4**, 025603 (2020).

[71] T. Mäkinen, A. D. S. Parmar, S. Bonfanti, and M. J. Alava, Data related to paper "Growth and prediction of plastic strain in metallic glasses" [Data set], Zenodo (2026), doi:10.5281/zenodo.18299181.